Available online at www.sciencedirect.com
ScienceDirect
Polymer 48 (2007) 205–219
polymer
www.elsevier.com/locate/polymer

Thermal and viscoelastic structure–property relationships of model comb-like poly(*n*-butyl methacrylate)

Johannes J. Vosloo [a], André J.P. van Zyl [b], Timothy M. Nicholson [c], Ronald D. Sanderson [c], Robert G. Gilbert [a,*]

[a] *Key Centre for Polymer Colloids, School of Chemistry F11, The University of Sydney, Sydney, NSW 2006, Australia*
[b] *UNESCO Associated Centre for Macromolecules and Materials, Department of Chemistry and Polymer Science, University of Stellenbosch, Private Bag X1, De Beers Street, Matieland 7602, South Africa*
[c] *Centre for High Performance Polymers, Division of Chemical Engineering, University of Queensland, St Lucia, QLD 4072, Australia*

Received 28 July 2006; received in revised form 3 November 2006; accepted 8 November 2006
Available online 4 December 2006

Abstract

A range of comb polymers of poly(*n*-butyl methacrylate), where the degree of polymerization (DP) of both the backbone and branches was controlled using RAFT-mediated free-radical polymerization, was synthesized using the method of Vosloo et al. [Macromolecules 2004;37: 2371]. Individual architectural parameters (branch length, branch number and DP of the comb backbone) of these relatively monodisperse samples were systematically varied in order to study the impact of each structural parameter on the thermal and rheological properties of the resulting comb polymers. Differential scanning calorimetry showed lower glass transition temperatures for the comb polymers compared to the original linear backbones. There were negligible differences in glass transition temperatures between comb polymers containing branches of different lengths, and between comb polymers containing backbones of narrow and of broad molecular weight distributions. These observations suggest that because the comb polymers are very tightly spaced, the branches act in the same way as long chain polyBMA. Viscoelastic properties of the comb polymers were investigated using dynamic mechanical analysis, using time–temperature superposition to extend the rheological data over a wide frequency range. Major differences in the viscoelastic responses of the original linear backbones and the comb polymers were observed, which were explained in terms of arm retraction/relaxation leading to tube dilation. All comb polymers showed viscoelastic responses that are characteristic of combs, but differences in responses due to changes in branch length and branch number were difficult to detect. This was mainly due to the relatively high number of branches, whose retractions occurred over a broad frequency range, and thus dominated the observed changes in moduli, thereby possibly masking subtle differences in responses.

Keywords: Viscoelastic properties; Branching; RAFT

1. Introduction

Branching can have significant effects on the rheological and other properties of a polymer. Correlating the molecular structure of branched polymers with material properties (mechanical, optical, electrical, etc.) has long been a challenge. Many common branched polymers (e.g. butyl acrylate) are synthesized using free-radical polymerization. Studying structure–property relationships in branched systems is no easy task, since branching in free-radical polymerization systems is random in both degree of polymerization of the branch and branching frequency, and also typically results in branches on branches on branches….

The development of controlled free-radical polymerization techniques has enabled, for the first time, the synthesis of polymers by free radical polymerization with controlled and predictable architectures [1–3]. The result of this new capability was that the contribution of a single structural parameter to material properties could be isolated and studied by synthesizing near identical structures (e.g. star or graft polymers) in

* Corresponding author. Tel.: +61 2 9351 3366; fax: +61 2 9351 8651.
E-mail address: gilbert@chem.usyd.edu.au (R.G. Gilbert).

0032-3861/$ - see front matter © 2006 Elsevier Ltd. All rights reserved.
doi:10.1016/j.polymer.2006.11.024

successive batches, while systematically changing this single structural parameter. Rigorous studies of structure–property correlations ultimately require libraries consisting of compounds for which every architectural parameter has been unambiguously quantified. This, in turn, has stimulated the development and refining of analytical instruments and techniques such as the use of multiple detectors with size-exclusion chromatography and multi-dimensional chromatography [4–6].

This study examines structure–property correlations in a special type of branched structure: comb polymers. Differential scanning calorimetry (DSC) and dynamic mechanical analysis (DMA) offer possibilities of probing the thermal and mechanical properties of these comb polymers. DMA measurements, in conjunction with the time–temperature superposition principle, can show changes in mechanical properties over extremely wide time scales [7]. Apart from numerous reports concerning the thermal and electrochemical properties of liquid crystalline and electrolyte comb polymer structures, there is a limited number of published papers that deal with the viscoelastic structure–property relations of comb polymers [8–12].

In the present paper, the correlation between molecular structure and properties was studied by synthesizing a range of controlled comb-like poly(BMA-*co*-NAS-*graft*-BMA), where NAS is *N*-acryloxysuccinimide, systematically varying the branch length, branch number and molecular weight distribution of the backbone. The ‘‘grafting from’’ approach [13–17] in conjunction with reversible addition-fragmentation chain transfer (RAFT) [18], was used to synthesize these precise comb polymers, as shown in Scheme 1. Details of the synthesis have been given previously [19]. The ‘‘grafting from’’ approach has been successfully employed in various polymerization systems to obtain comb polymers and other molecular structures. These systems include ATRP and group transfer [20,21], nitroxyl/alkoxyamine [22,23], urethane [24], peroxide [25,26] and RAFT-based systems [17,27–29]. A common problem reported when using the ‘‘grafting from’’ approach, however, was broad and complex (multimodal) molecular weight distributions of the final comb polymers. In free-radical based ‘‘grafting from’’ systems, especially such multimodal molecular weight distributions are a direct result of the complexities inherent in the mechanism when the second-stage chain growth is initiated from appropriately functionalized polymer chains or surfaces. In RAFT-based ‘‘grafting from’’ systems, the possible fates of propagating radicals during the second stage of comb synthesis can become quite diverse, as shown in Scheme 2.

Scheme 2 shows a number of products that may form during the final stage of the ‘‘grafting from’’ approach in a RAFT-based system. In any RAFT system where polymers are synthesized through successive polymerization reaction steps, primary free radicals are usually required to reinitiate the addition–fragmentation process at the onset of each

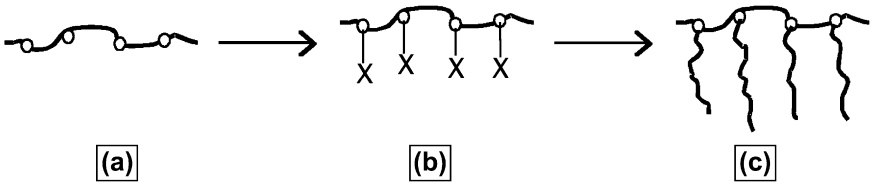

Scheme 1. The ‘‘grafting from’’ approach as employed here: (a) synthesis of linear polymer chains containing functional groups [poly(BMA-*co*-NAS)], (b) immobilization of RAFT agents (designated by X) onto functional sites to yield poly(BMA-*co*-NAS-*graft*-RAFT agent) and (c) branch growth from the immobilized RAFT agents to yield comb-like poly(BMA-*co*-NAS-*graft*-BMA).

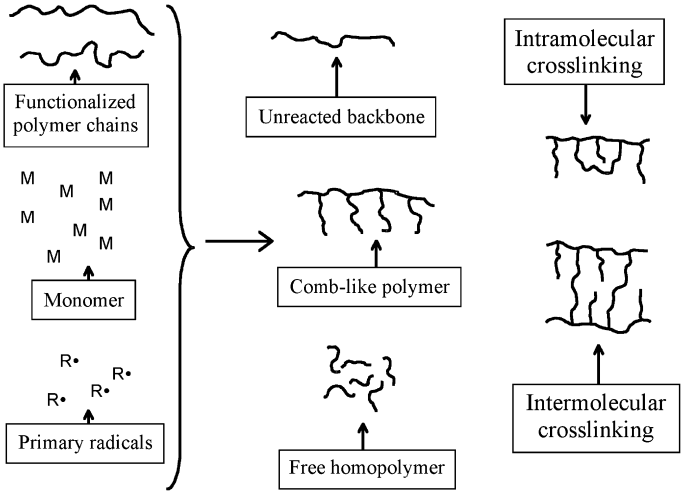

Scheme 2. Possible products that may form during the final phase of the ‘‘grafting from’’ approach in a RAFT-based system – leading to complex hydrodynamic volume distributions.

step. In the procedure described in Scheme 2, an inevitable consequence of adding primary free radicals (R•) will be the formation of free homopolymer chains. This happens through the polymerization of the additional monomer (M) needed for branch growth. Also, some of the original backbone polymer chains might only be partially functionalized (in terms of immobilized RAFT agents) or not functionalized at all for branch growth, leading to those chains remaining as is. Finally, the desired comb polymers can undergo inter- and intramolecular crosslinking reactions through the combination of growing side chains, since the propagating centers are located on the chain ends of the side chains. This leads to the formation of high molecular weight species, and even the formation of insoluble, highly crosslinked components.

The aim of the present paper thus required combining the relative experimental simplicity of the ''grafting from'' approach with the robustness of the RAFT process, while minimizing the contribution of unwanted side reactions inherent to the final stage of the synthesis. To check on whether this aim was achieved, every architectural parameter of the comb polymers was characterized individually. The linear poly(BMA-*co*-NAS) chains that served as backbones were characterized using SEC–MALLS and the number of branches were determined using ^{1}H NMR spectrometry [19]. Branches were cleaved using a transesterification procedure and directly analyzed using SEC–MALLS. This enabled the isolation of the impact of each of these architectural parameters on the mechanical and thermal properties.

2. Experimental

2.1. Materials used

Butyl methacrylate (BMA, Aldrich, 99%) was purified by using an inhibitor removal column. Azobisisobutyronitrile (AIBN, Delta Scientific, 98%) was recrystallized from methanol. Tetrahydrofuran (THF, HPLC grade) was used as received.

2.2. Comb polymer synthesis

The synthesis procedure used to prepare the linear poly(BMA-*co*-NAS-*graft*-RAFT agent) and comb-like poly-(BMA-*co*-NAS-*graft*-BMA) is described in detail elsewhere [19]. The only notable deviation from the synthesis as described in this reference was the use of butyl 2-(2-hydroxyethylamino)-1-methyl-2-oxoethyl trithiocarbonate (**1**) (see Scheme 3) as the immobilized RAFT agent instead of the benzyl analog (**2**) in the preparation of poly(BMA-*co*-NAS-*graft*-RAFT agent) from poly(BMA-*co*-NAS). The RAFT agent used for backbone poly(BMA-*co*-NAS) synthesis was 2-cyanopropyl dithiobenzoate (**3**).

2.3. Cleaving of branches from poly(BMA-co-NAS-graft-BMA)

Branches (side chains) were cleaved using an acid-catalyzed transesterification procedure [30]. It was important to use concentrated acid, since the water in diluted acid can lead to the formation of acrylic acid and methacrylic acid units in the polymer chains. These side reactions render the polymer products insoluble in THF. The reaction was performed at 90 °C for 5–7 days and the final product was precipitated in methanol. After isolation, the product was washed with methanol and dried in vacuo. A typical reaction mixture contained poly(BMA-*co*-NAS-*graft*-BMA) (0.259 g), THF (12.0 mL), butan-1-ol (30.0 mL) and fuming sulfuric acid (10 drops).

2.4. Size-exclusion chromatography analysis

Samples were prepared for size-exclusion chromatography (SEC) analysis by drying the polymer in vacuo and redissolving ca. 1–3 mg of the polymer in 1 mL of THF. SEC–DRI analyses were carried out using a Shimadzu system fitted with a series of Waters columns (HR4, HR3 and HR2). Molecular weight, or apparent molecular weight for branched samples, was determined from refractive index data analyzed with Polymer Laboratories Cirrus software. The flow rate was 1 mL min^{-1} and 45 min per sample. The system was calibrated using six polystyrene narrow molecular weight standards in the range of 580–2 × 10^6, supplied by Polymer Labs. All molecular weights were calculated relative to polystyrene.

It is important to realize that SEC separates a branched polymer by hydrodynamic volume V_h, not by molecular weight. As is well known but too often unappreciated, there is no unique relationship between V_h and M for branched systems, and the best that SEC can give, even with multiple detection, is an average molecular weight of the range of chains with that particular elution volume [31].

Fortunately, for the comparative characterization purposes of the present paper, it is unnecessary to present the data in terms of the unfamiliar quantity $\log V_h$, and so the data are presented in terms of $\log M$ (apparent), where M (apparent) is the molecular weight of a linear polystyrene chain with the same hydrodynamic volume as that of the (branched) sample [32].

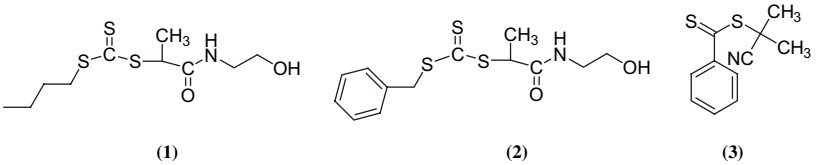

Scheme 3. Different RAFT agents involved in the synthesis of poly(BMA-*co*-NAS) and poly(BMA-*co*-NAS-*graft*-BMA): butyl 2-(2-hydroxyethylamino)-1-methyl-2-oxoethyl trithiocarbonate (**1**), benzyl 2-(2-hydroxyethylamino)-1-methyl-2-oxoethyl trithiocarbonate (**2**) and 2-cyanopropyl dithiobenzoate (**3**).

Multi-angle laser light scattering (MALLS) in conjunction with SEC was used to determine absolute weight-average molecular weight ($\overline{M}_w$) as a function of elution volume (and hence of hydrodynamic volume). The SEC instrument in the SEC–MALLS setup consists of a Waters 717_{plus} Autosampler, Waters 600E System Controller and a Waters 610 fluid unit. A Waters 410 differential refractometer was used at 30 °C as detector. Tetrahydrofuran (HPLC grade) sparged with IR-grade helium was used as eluent at a flow rate of 1 mL min^{-1}, giving a runtime of 30 min per sample. The column oven was kept at 30 °C and the injection volume was 100 μL. Two PLgel 5 μm Mixed-C columns and a pre-column (PLgel 5 μm Guard) were used in series. The system was calibrated using narrow molecular weight polystyrene standards ranging from 200–2×10^6, supplied by Polymer Labs. The MALLS instrument in the SEC–MALLS setup was a DAWN DSP-F 18-angle light scattering detector (Wyatt Technology). The wavelength of the laser was 632.8 nm and the collection interval was 1 s. ASTRA software (Wyatt Technology) was used for data collection and processing. The change in refractive index with respect to concentration (d*n*/d*c*) was determined off-line using a scanning interferometric refractometer (SCANREF) with a laser wavelength of 633 nm, and was found to be 0.083 mL g^{-1} for poly(BMA-*co*-NAS) (containing roughly 20% NAS, synthesized using RAFT agent **3**) and 0.074 mL g^{-1} for poly(*n*-butyl methacrylate) that was synthesized by conventional free-radical polymerization. For the construction of d*n*/d*c* curves, 6–10 different sample concentrations ranging from 0 to 10 mg mL^{-1} were used. Samples of eluent without polymer were also injected in order to construct an adequate baseline.

2.5. Differential scanning calorimetry (DSC) analysis

DSC thermograms were recorded on a 2920 MDSC differential scanning calorimeter (Thermal Advantage Instruments). Data were analyzed using Thermal Advantage Universal Analysis 2000 software. Before analysis, each sample (typically 6–10 mg) was placed in an open aluminum pan and heated to 140 °C to ensure that any atmospheric moisture, residual solvent and monomer were evaporated. After cooling, the pan was sealed and subjected to a heating/cooling/heating cycle to remove any thermal history. Heating/cooling/heating cycles consisted of first heating the sample to 200 °C at a rate of 5 °C min^{-1}, then cooling to −60 °C at a rate of 5 °C min^{-1} and finally heating to 200 °C at a rate of 5 °C min^{-1}.

2.6. Dynamic mechanical analysis (DMA)

DMA measurements were recorded on a Rheometric Scientific DMTA IV dynamic mechanical analyzer. Data were analyzed using RSI Orchestrator software. Sample films for DMA analysis were prepared by dissolving 0.5–0.7 g polymer in ca. 20 mL solvent (acetone for linear polymers and 1:1 dichloromethane:ethanol mixture for branched polymers) and casting each of the solutions in separate aluminum weighing pans. Uniform film formation was achieved by adding additional solvent to the samples after initial drying and evaporating the solvent at a controlled rate. This procedure was repeated until clear films of uniform thickness (0.22–0.35 mm) were obtained. Tensile tests were conducted on clamped square films with the instrument in the rectangular tension/compression mode. Strain sweeps were conducted at 20 °C to determine the linear region of the viscoelastic response. This was checked for all samples, with 0.02% selected as an appropriate strain.

Time–temperature superpositioning (TTS), in conjunction with conventional DMA measurements, offers the possibility of observing the mechanical responses of materials over extremely wide frequency ranges. This is achieved through the construction of master curves [7] and has been shown to be reliable for relatively monodisperse samples [33]. The underlying principle behind TTS is that any material property (creep behavior, storage and loss moduli, etc.) will exhibit the same trend over a wide frequency range as it would over a wide temperature range. Master curves were constructed by overlapping the different data sets by horizontal shifting, relative to a stationary reference temperature (T_r) data set.

Temperature sweeps at 1 Hz were done from −100 °C to 100 °C at a heating rate of 5 °C min^{-1}. In order to do time–temperature superposition, frequency sweeps (0.01–100 Hz) were performed at different temperatures with 20 °C intervals to ensure sufficient overlapping of the data. The temperatures were ranged from −80 °C to 80 °C, depending on the integrity of the sample. Horizontal shifting of data sets was done by inspection until sufficient overlapping was obtained. Vertical shifting of data sets (up to a maximum of 20%) was done to compensate for effects due to thermal expansion of the tools. The reference temperature for superpositioning was 0 °C.

3. Results and discussion

3.1. Comb polymer synthesis and analysis

Three different series of comb-like poly(BMA-*co*-NAS-*graft*-BMA) were prepared. In each of these series, only one architectural parameter was varied at a time. The following parameters were systematically varied.

(1) Branch length: this was achieved by preparing identical poly(BMA-*co*-NAS) that contained the same amount of immobilized RAFT agents, and growing side chains of different lengths from these polymers. Different branch lengths were obtained by adding BMA in different stoichiometric quantities with respect to the amount of immobilized RAFT agents on the poly(BMA-*co*-NAS-*graft*-RAFT agent).
(2) Branch number: this was varied by preparing identical poly(BMA-*co*-NAS), and controlling the extent of RAFT agent immobilization on the poly(BMA-*co*-NAS). Side chains of similar lengths were subsequently grown from the different poly(BMA-*co*-NAS-*graft*-RAFT agent), yielding comb polymers differing only with respect to the number of branches.

(3) Molecular weight distribution of the comb backbone: this series was created by synthesizing poly(BMA-*co*-NAS) of comparable molecular weights under RAFT and conventional free-radical polymerization conditions. The different poly(BMA-*co*-NAS) linear chains were subsequently functionalized (in terms of immobilized RAFT agents) to similar degrees. Finally, side chains were grown to similar lengths from the different poly(BMA-*co*-NAS-*graft*-RAFT agent).

Characterization results for the comb polymers described above are shown in Table 1. Fig. 1 shows, as a typical example of the final comb polymers obtained, the hydrodynamic volume distributions (expressed in terms of apparent molecular weight) of the branched polymer, poly(BMA-*co*-NAS-*graft*-BMA), differing only with respect to the branch (side chain) lengths; the abscissa of Fig. 1, being log(styrene equivalent apparent molecular weight), is related to log V_h by a simple linear transformation. These hydrodynamic volume distributions of the final comb polymers were monomodal – indicating that unwanted side reactions (as shown in Scheme 2) were largely avoided. The synthesis technique used to obtain these controlled comb polymers consistently yielded polymers with narrow and monomodal distributions – indicating the robustness and reliability of the technique [19].

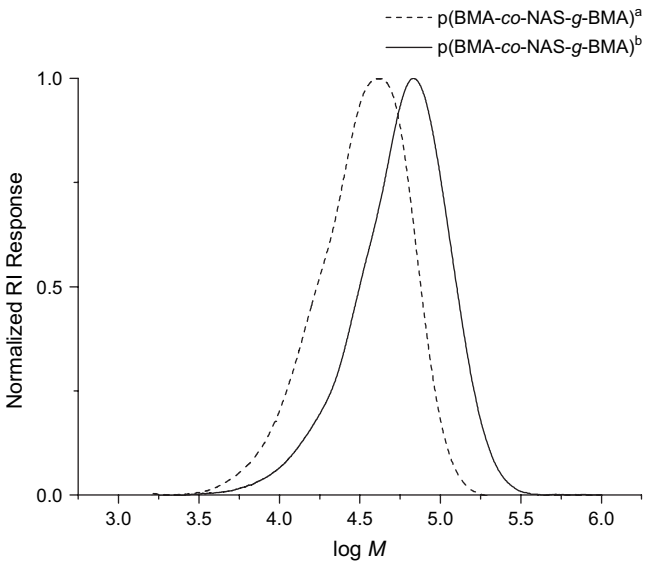

Fig. 1. Apparent molecular weight distributions of poly(BMA-*co*-NAS-*graft*-BMA) with identical original backbones, but different branch lengths, as obtained using a DRI detector: (a) $\overline{M}_n$ = 19 500, PDI = 1.54, targeted branch $\overline{M}_n \sim 10\,000$ and (b) $\overline{M}_n$ = 32 800, PDI = 1.61, targeted branch $\overline{M}_n \sim 30\,000$. For these branched polymers, the ordinate, log(apparent molecular weight), refers to the molecular weight of styrene with the same hydrodynamic volume as the sample in that elution slice.

The poly(BMA-*co*-NAS-*graft*-BMA) samples depicted in Fig. 1 were originated from the same poly(BMA-*co*-NAS) backbone ($\overline{M}_n = 5.8 \times 10^4$ as determined using the same calibrated DRI detector). The apparent molecular weights (and hence hydrodynamic volumes) for the poly(BMA-*co*-NAS-*graft*-BMA) samples were seemingly lower than those of the original poly(BMA-*co*-NAS) backbone; this qualitative observation is independent of the calibration with linear polystyrene standards. This SEC behavior of branched polymers, which at first glance appears abnormal, is not uncommon and numerous references to this phenomenon exist [34–36]. "Abnormal" SEC behavior of the branched polymers can be a combination of a number of factors, and is not yet fully understood [4,5,31]. It has been reported that the hydrodynamic volumes of branched polymers can be smaller than those of linear polymer chains for the same molecular weight [4]. Moreover, different types of entanglements of branched polymers with the column gel can lead to retardation during the SEC process, especially in the case of randomly branched polymers [5]. Further, it is possible that the comb nature of the branched polymers synthesized here (illustrated later in this paper) gives them an aspherical average shape which slows elution through the pores of the column compared to a randomly branched or linear polymer. These effects could lead to an increase in elution time and an exaggerated tailing in the hydrodynamic volume distribution.

Multi-angle laser light scattering (MALLS) was also used in conjunction with SEC to obtain additional data for the comb-like poly(BMA-*co*-NAS-*graft*-BMA). Table 1 shows the comparison between SEC–MALLS and SEC–DRI data for different poly(BMA-*co*-NAS-*graft*-BMA) samples.

It is essential to be aware that SEC with only DRI and MALLS detections cannot give a value of $\overline{M}_n$ for a branched polymer. MALLS measures the absolute value of $\overline{M}_w$ in each elution slice, but the reduction of MALLS and DRI data to a value of the number-average molecular weight $\overline{M}_n$ of the whole distribution requires additional data [31]. While

Table 1
SEC characterization data for different poly(BMA-*co*-NAS-*graft*-BMA) samples

Sample (percent branching in parentheses)	Backbone		Resulting comb polymer				Branch length
	MALLS		DRI		MALLS		MALLS
	$\overline{M}_n$	PDI	Apparent $\overline{M}_n$	Apparent PDI	Apparent $\overline{M}_n$	Apparent PDI	$\overline{M}_n$
Poly(BMA-*co*-NAS-*graft*-BMA) (~20%)	9.5×10^4	1.32	2.0×10^4	1.54	9.0×10^4	1.21	9.9×10^3
Poly(BMA-*co*-NAS-*graft*-BMA) (~20%)	9.5×10^4	1.32	3.3×10^4	1.61	1.1×10^5	1.38	2.5×10^4
Poly(BMA-*co*-NAS-*graft*-BMA) (~11%)	9.5×10^4	1.32	1.28×10^5	2.05	2.7×10^5	1.44	(2.5×10^4)
Poly(BMA-*co*-NAS-*graft*-BMA) (~7%)	5.7×10^4	1.71	6×10^4	1.92	1.3×10^5	1.32	(2.5×10^4)

Amount of branching, branch length and backbone length are shown as well as a comparison between DRI and SEC–MALLS data for the resulting comb polymers. For the branched (comb) polymers, data are in terms of apparent molecular weight relative to linear polystyrene. Because DRI and MALLS detection alone cannot yield true values for branched polymers, these apparent values are only for qualitative comparison. PDI = (apparent) polydispersity index = $\overline{M}_w/\overline{M}_n$.

under certain circumstances the number distribution can be obtained by combining refractive index and viscometric detectors [37,38], this is not the case with a highly branched comb polymer such as the present, where the relation between viscosity, molar mass and branching architecture does not follow the Flory result (or, to be more precise, the hydrodynamic volume inferred by combining data from viscometric and refractive index detectors does not have the same value of the Flory–Fox constant Φ as that for linear or lightly branched polymers [31]). Apparent values of $\overline{M}_n$ relative to polystyrene are reported in Table 1 for qualitative purposes. The apparent number-average molecular weights of the comb polymers obtained through SEC–MALLS measurements were closer to the expected absolute molecular weights than the molecular weights obtained by SEC–DRI, but were still lower than expected; however, in view of the remarks above, no meaningful conclusion can be drawn from this observation.

Fortunately, inferences as to the molecular weight of the comb polymers can be drawn without $\overline{M}_n$ data. This is because, upon completion of each reaction step involved in the step-wise synthesis of the comb polymers, the backbone length and molecular weight distribution of the branches (branch number and branch length) could be quantified as follows.

The side chains of the comb-like poly(BMA-*co*-NAS-*graft*-BMA) bonded to the main backbone via ester bonds were directly analyzed by performing an acid-catalyzed transesterification procedure, as shown in Scheme 4 [30]. Ester bonds are very stable and the cleaving reaction required extreme reaction conditions (90 °C for ~7 days). A typical result of this procedure performed on poly(BMA-*co*-NAS-*graft*-BMA) is shown in Fig. 2. This shows the evolution of a second population of chains, indicating that the procedure was successful. The relative intensity of the branch population was low, which could be ascribed to a number of possible reasons. These include the low number (~7% in case depicted in Fig. 2) of branches in the poly(BMA-*co*-NAS-*graft*-BMA), the equilibrium nature of an esterification reaction and finally, steric hindrance considerations. The transesterification procedure was carried out with butan-1-ol (which simultaneously acted as reaction solvent), implying that cleaved side chains were

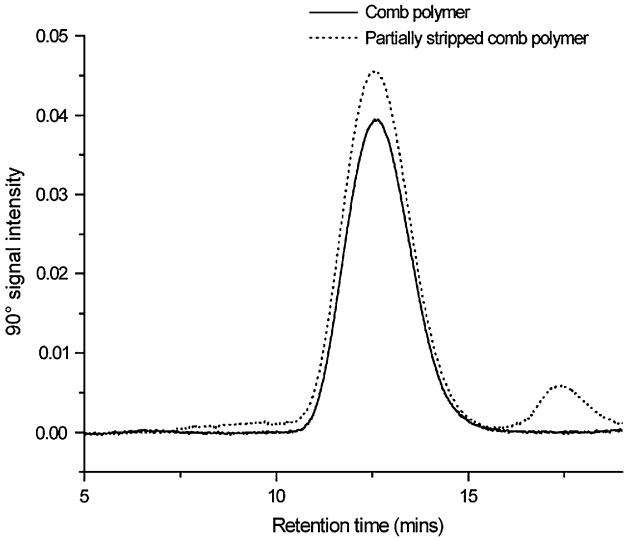

Fig. 2. Apparent molecular weight distributions illustrating a typical result of a transesterification procedure performed on poly(BMA-*co*-NAS-*graft*-BMA) to enable direct observation of side chains. The signal intensities of the detector set at 90° in the MALLS instrument are shown.

replaced by butyl groups. The cleaving (transesterification) reaction of the side chains would have had strong competition from the transesterification of the butyl-ester groups contained in every BMA repeat unit along the main chains and side chains. This competition would have translated into butyl groups (from the solvent) replacing butyl groups (contained in the polymers). This side reaction has no net effect, but the esterification of the small butyl groups is significantly easier than the cleaving of the large side chains, leading to severe competition. The fact that the side chains were present in significantly lower concentrations than the butyl-ester groups would only have increased the severity of the competition. These factors, coupled with the fact that esterification procedures are equilibrium reactions, probably led to poly(BMA-*co*-NAS-*graft*-BMA) samples only being partially stripped of side chains during the transesterification procedure. It was, however, not necessary for all branches to be cleaved, since side chains were not expected to be cleaved

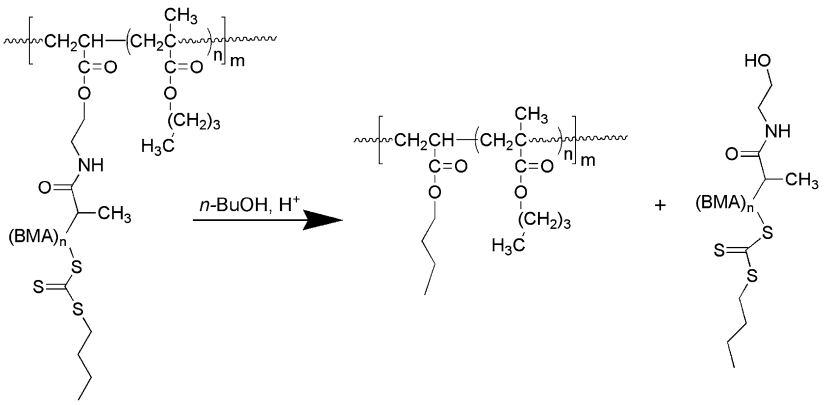

Scheme 4. Transesterification procedure used to analyze side chains of poly(BMA-*co*-NAS-*graft*-BMA) directly.

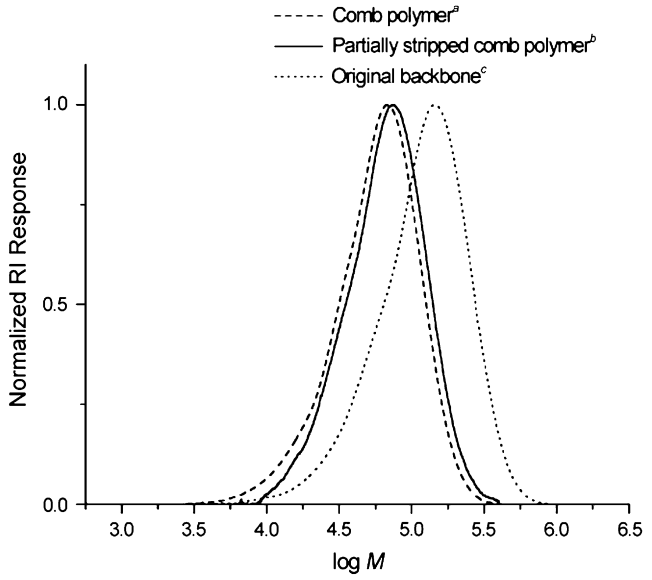

Fig. 3. Illustration of the abnormal SEC behavior of branched polymers. Apparent molecular weight distributions of: (a) comb-like poly(BMA-*co*-NAS-*graft*-BMA) $\overline{M}_n = 3.3 \times 10^4$, PDI = 1.61, (b) poly(BMA-*co*-NAS-*graft*-BMA) partially stripped of side chains $\overline{M}_n = 4.1 \times 10^4$, PDI = 1.45 and (c) original poly(BMA-*co*-NAS) backbone $\overline{M}_n = 5.8 \times 10^4$, PDI = 1.91 as obtained using a DRI detector.

preferentially with respect to each other. Any population of cleaved branches would thus be representative of the side chains contained in the poly(BMA-*co*-NAS-*graft*-BMA), given a sufficiently long reaction period for the transesterification procedure.

SEC analysis of poly(BMA-*co*-NAS-*graft*-BMA) polymers that were partially stripped of the side chains served as an additional illustration of the abnormal SEC behavior of branched polymers. Fig. 3 shows three (apparent) molecular weight distributions that were obtained using a DRI detector: (a) comb-like poly(BMA-*co*-NAS-*graft*-BMA), (b) the same poly(BMA-*co*-NAS-*graft*-BMA) that had been partially stripped of the side chains and (c) the linear poly(BMA-*co*-NAS) that served as backbone for the poly(BMA-*co*-NAS-*graft*-BMA). The characterization data accompanying Fig. 3 suggest that the apparent molecular weights of the polymers under consideration increase as the amount of branching decreases. This is ascribed to an artifact of the retardation that branched (especially comb) polymers can experience during SEC. The apparent increase in molecular weight is due to the fact that the polymers with fewer branches experience less retardation and therefore elute faster, thereby ''increasing'' the molecular weight: that is, SEC separation is non-ideal. Of the three examples, the linear poly(BMA-*co*-NAS) eluted fastest and was therefore assigned the highest apparent molecular weight.

3.2. Molecular structure

The comb polymers under consideration have a brush-like character. Ball-and-stick and atomistic space-filling images are shown in Fig. 4, generated by using the Accelrys Material Studio software package and the PCFF (polymer consortium force field) model [39]. These figures permit comparison of the spatial structure of linear poly(*n*-butyl methacrylate) with that of comb-like poly(BMA-*graft*-BMA). These images show a significant measure of steric hindrance in the linear polymer molecule. The steric hindrance increases significantly when side chains are added to the linear polymers. The comb polymers depicted in this figure contain branches of only 10 repeat units long, while the actual comb polymers under consideration in this study contained branches of roughly 69 and 178 repeat units long, respectively. These branches will experience even greater constraints with respect to general mobility and motions. All these constraints and barriers to motion and translation will contribute to the thermal and mechanical properties of these novel polymers.

3.3. Thermal properties

Figs. 5–7 show the effect of various structural parameters on the thermal properties of the comb polymers. Fig. 5 shows the effect of branch (side chain) length on the glass transition temperature (T_g) of the polymers. Fig. 6 shows the effect of the amount of branching and Fig. 7 shows the effect of the molecular weight distribution of the backbone chains of the comb polymers on the T_g of the different polymers. The thermograms show a significant decrease in T_g when going from linear poly(BMA-*co*-NAS) to comb-like poly(BMA-*co*-NAS-*graft*-BMA). The T_g of poly(*n*-butyl methacrylate) is in the range of 20–25 °C [40], which is close to the measured T_g of the combs. The poly(BMA-*co*-NAS) will have a different T_g since it is a different material altogether. There was no significant difference in T_g between the two combs having different branch lengths. The difference in T_g between combs having different amounts of branching was barely significant, considering the difference in the amount of branching (20% vs 11%). The molecular weight distribution of the backbone of the comb polymers also had no impact on the T_g.

The structural nature of these comb polymers, as shown in Fig. 4, is such that many different molecular and sectional translational motions and modes can be simultaneously at work to ultimately result in the observed T_g. Bearing in mind that the thermal properties of these types of polymers have not yet been rigorously studied, three postulates are put forward in order to explain the trends observed in Figs. 5 and 6.

The first postulate is an attempt to ascribe the decrease in T_g in going from linear chains to comb polymers to the presence of low molecular weight species (i.e. the branches). This postulate infers that the branches dominate the value of T_g. Lu and Jiang [41] have reported a method to predict the dependence of T_g on the number-average molecular weight, yielding the following set of expressions:

$$T_g = \frac{69.5nT_{g\infty}}{69.5n + T_{g\infty}F(y)} \quad (1)$$

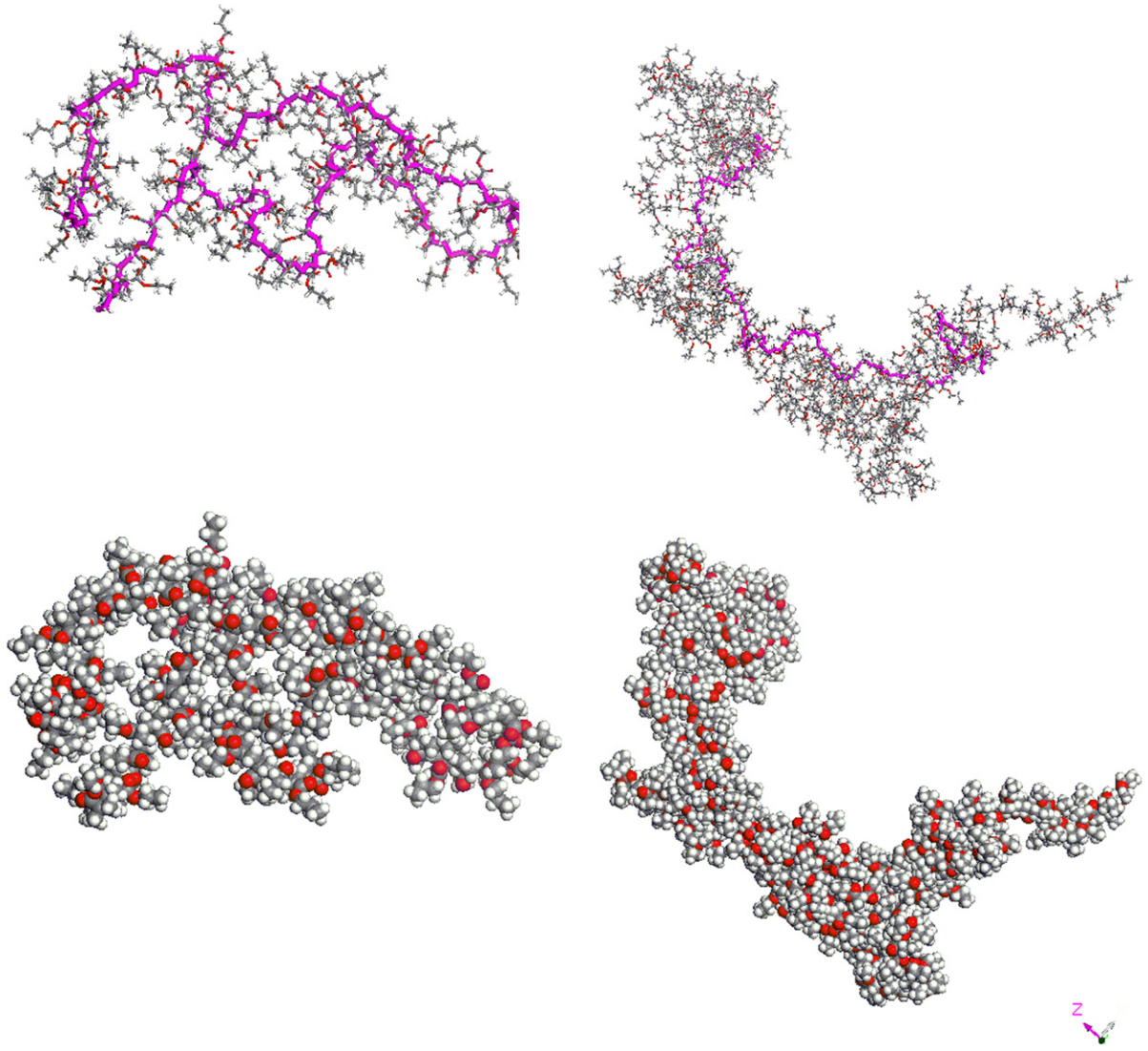

Fig. 4. Left-hand images: ball-and-stick and space-filling images of linear poly(*n*-butyl methacrylate) with 100 repeat units. Right-hand images: ball-and-stick and space-filling images of comb-like poly(*n*-butyl methacrylate) with a backbone of 100 repeat units containing 20% branching with each branch being 10 repeat units. The backbone is shown in dark in the ball-and-stick images.

$$\text{with } F(y) = 1 - 3y + 6y^2 - 6y^3\left[1 - \exp\left(-\frac{1}{y}\right)\right] \tag{2}$$

$$\text{and } y = \frac{T_{g\infty}}{139n\sin^2(\theta/2)} \tag{3}$$

Here n is the number-average degree of polymerization, $T_{g\infty}$ is the glass transition temperature in Kelvin at infinite degree of polymerization and θ is the angle between successive backbone bonds (usually approximated as the tetrahedral angle). For the linear poly(BMA-*co*-NAS) under consideration, n was calculated by using the number-average molecular weight of 9.5×10^4, and by recalling that poly(BMA-*co*-NAS) under discussion contained roughly 20% NAS monomer ($\sim$169 g mol^{-1}) and 80% BMA monomer ($\sim$143 g mol^{-1}). This yielded a value of 640 for n. The dependence of T_g of the backbone poly(BMA-*co*-NAS) on the degree of polymerization, as described by this model, is shown in Fig. 8. This model predicts that $T_{g\infty}$ of the poly(BMA-*co*-NAS) sample is 51 °C, using the measured T_g of 49 °C. Fig. 9 shows the results of the same calculations for poly(*n*-butyl methacrylate) and a $T_{g\infty}$ of 25 °C. This gives T_g's of $\sim$10 °C and $\sim$18 °C for poly(*n*-butyl methacrylate) chains of 9.9×10^3 (length of the short branches) and 2.5×10^4 (length of the long branches), respectively. These predicted T_g's are significantly lower than the measured T_g's for the comb polymers, as shown in Fig. 8, which are very close to the $T_{g\infty}$ value for poly(*n*-butyl methacrylate). This is a strong indication that the modes controlling the value of the T_g for the combs are the same modes that control the T_g of long chain poly(*n*-butyl methacrylate). This is probably because the short branch chains are not able to move in the same manner as free polymer chains, since one chain end will be attached to the comb

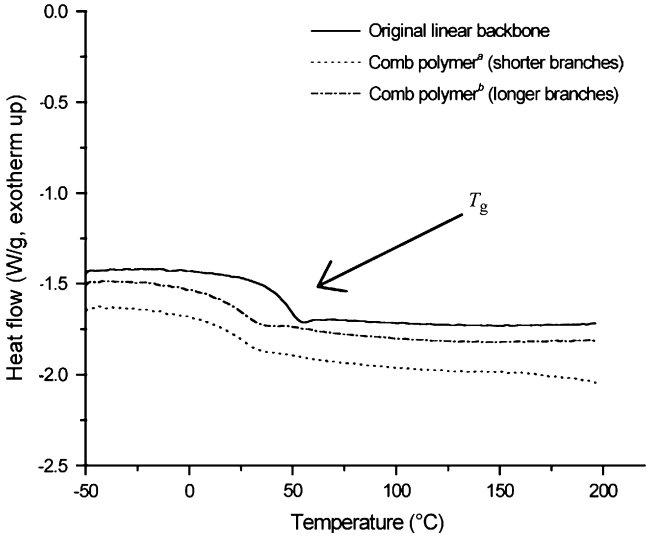

Fig. 5. DSC thermograms (final heating curves) showing the effect of branch length on the glass transition temperature T_g. Full line (—): original linear backbone poly(BMA-*co*-NAS) with $\overline{M}_n = 9.5 \times 10^4$ and $T_g = 49$ °C, (…, a): poly(BMA-*co*-NAS-*graft*-BMA) with branch $\overline{M}_n = 9.9 \times 10^3$ and $T_g = 26$ °C and (·–·–·, b): poly(BMA-*co*-NAS-*graft*-BMA) with branch $\overline{M}_n = 2.5 \times 10^4$ and $T_g = 25$ °C.

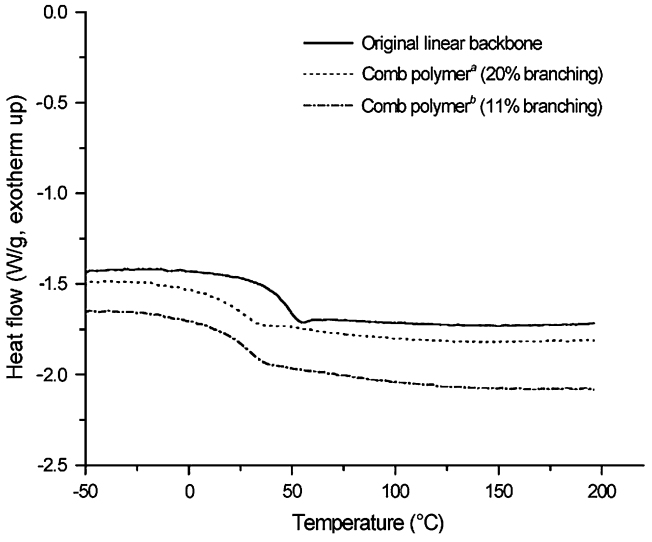

Fig. 6. DSC thermograms (final heating curves) showing the effect of the amount of branching on the glass transition temperature. Original linear backbone poly(BMA-*co*-NAS) with $\overline{M}_n = 9.5 \times 10^4$ and $T_g = 49$ °C, (a) poly(BMA-*co*-NAS-*graft*-BMA) containing 20% branching with branch $\overline{M}_n = 2.5 \times 10^4$ and $T_g = 25$ °C and (b) poly(BMA-*co*-NAS-*graft*-BMA) containing 11% branching with branch $\overline{M}_n \sim 2.5 \times 10^4$ and $T_g = 29$ °C.

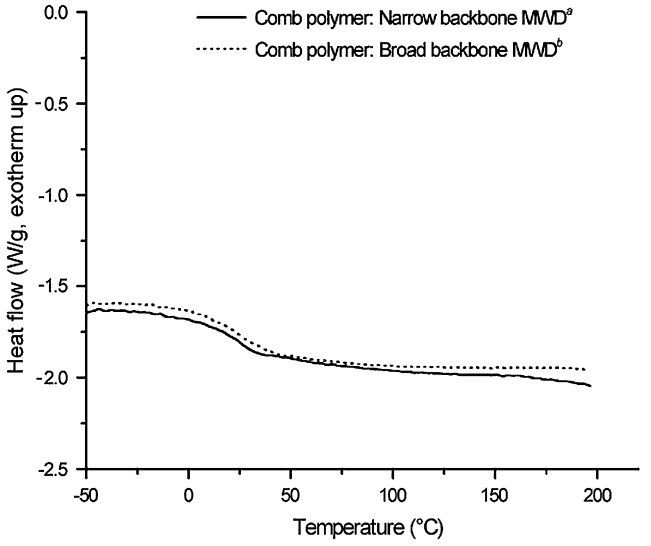

Fig. 7. DSC thermograms (final heating curves) showing the effect of the molecular weight distribution of the comb backbone on the glass transition temperature of the comb polymers. (a) Backbone $\overline{M}_n = 9.5 \times 10^4$, PDI = 1.32, branch $\overline{M}_n = 9.9 \times 10^3$ and $T_g = 26$ °C and (b) backbone $\overline{M}_n = 5.7 \times 10^4$, PDI = 1.71, branch $\overline{M}_n \sim 9 \times 10^3$ and $T_g = 24$ °C.

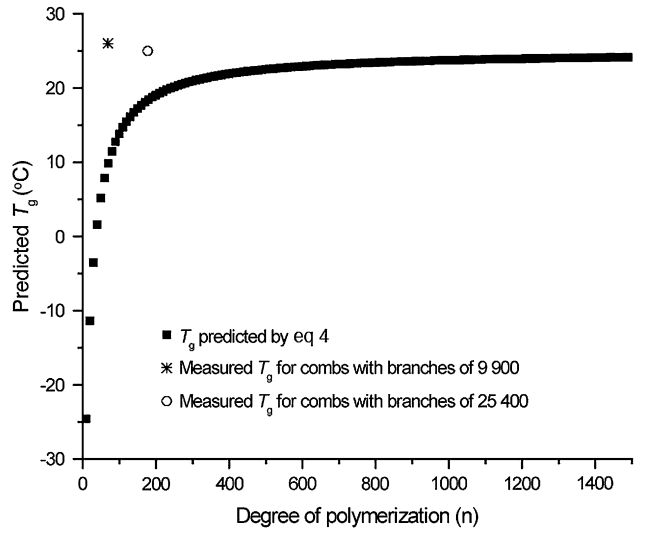

Fig. 8. Predicted values of T_g for poly(BMA-*co*-NAS) as a function of degree of polymerization, from Eq. (1) with $T_{g\infty} = 49$ °C. The predicted values are compared with the actual T_g's measured for the different comb polymers.

backbone. Steric hindrance due to neighboring branches will add further constraints to chain movements.

The second postulate involves the suggestion of an increase in free volume due to the increase in number of chain ends per polymer molecule in going from linear polymer chains to comb polymers. The branch ends will be highly mobile and their motions will cause an increase in free volume. This postulate includes the possibility that the branches can disrupt the packing of the polymer chains and, in doing so, effectively act as internal plasticizers. This explanation, however, is unlikely due to the small difference between the measured T_g's of the comb polymers containing 20% and 11% branching. One would expect a larger difference in T_g when roughly doubling the amount of branching. The small impact of the number of branches might also be related to the molecular structures depicted in Fig. 4. The branches in the comb polymers will find themselves in such a crowded environment that their mobility might be impaired.

The final postulate involves the contribution of the actual branch points. Although branch points add constraints to the

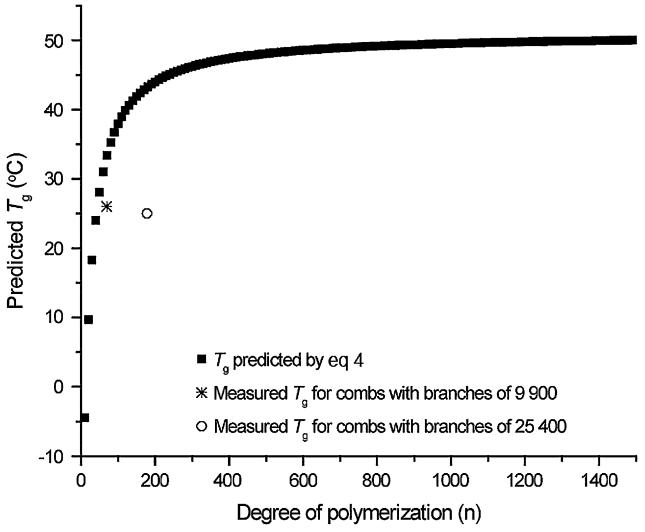

Fig. 9. As for Fig. 8 with $T_{g\infty} = 25\,^{\circ}C$ (the measured glass transition temperature for the comb polymers).

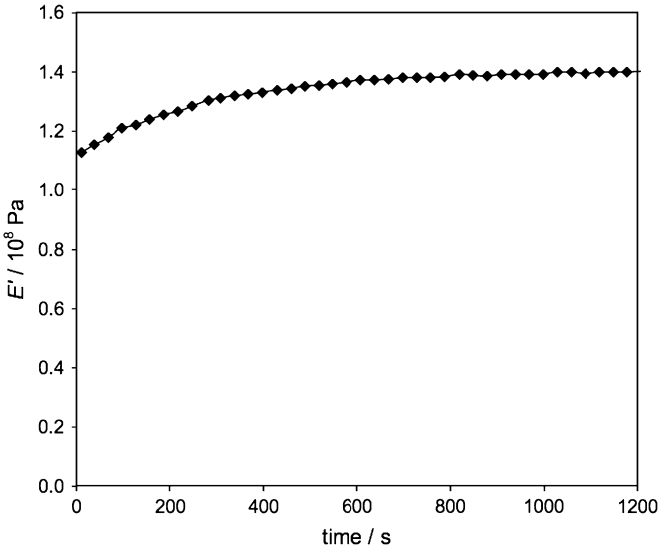

Fig. 10. Time dependence of storage modulus (E') at $-60\,^{\circ}C$ for a typical sample of comb polymer.

movements of the branches, some new translational modes might be added to the motions of the backbone.

In summary, since the measured T_g's of the combs are so close to the T_g of long chain polyBMA, the first postulate (i.e. that the branches act in the same way as long chain polyBMA because the combs are tightly packed together) is probably the main reason for the observed T_g's.

3.4. Mechanical properties

Before discussing the data of storage and loss moduli, it is essential to determine whether or not the conditions were such that these data actually refer to the equilibrium state of the samples. As the material is predominantly elastic, the storage modulus (E') data are the ones of relevance for testing this point. Fig. 10 shows the results of a scan of E' of a representative sample run at $-60\,^{\circ}C$. E' attains a constant value at $\sim$10 min and stays constant over the duration of this particular measurement (2 h), suggesting that the data used here, obtained with a hold time of 10 min and at temperatures which were for the most part above $-60\,^{\circ}C$, are indeed for a system at equilibrium.

Figs. 11–13 show the temperature dependence of the storage and loss (E'') moduli of the different comb polymers as compared to the original linear backbone polymers. Figs. 11 and 12 show that the comb polymers softened at a lower temperature than the original backbone polymers, consistent with the lower glass transition temperatures of the comb polymers as was shown by DSC analysis. The abrupt drop in moduli at $\sim 40\,^{\circ}C$ was often accompanied by sample elongation

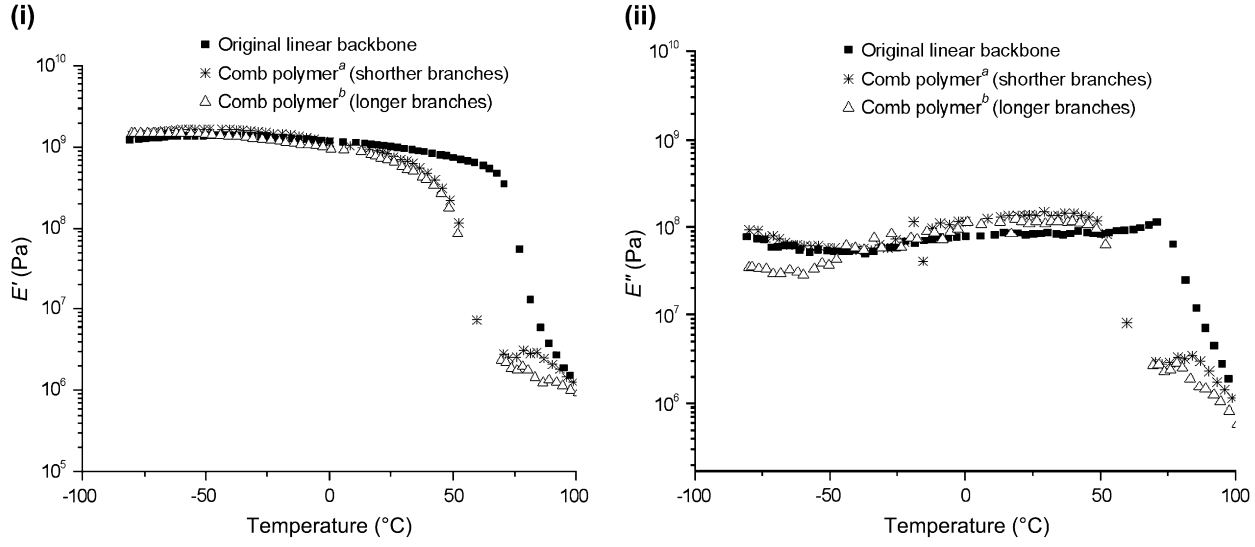

Fig. 11. Temperature dependences of (i) storage (E') and (ii) loss (E'') moduli of comb polymers with different branch lengths. Original linear backbone poly(BMA-*co*-NAS) with $\overline{M}_n = 9.5 \times 10^4$, (a) poly(BMA-*co*-NAS-*graft*-BMA) with branch $\overline{M}_n = 9.9 \times 10^3$ and (b) poly(BMA-*co*-NAS-*graft*-BMA) with branch $\overline{M}_n = 2.5 \times 10^4$.

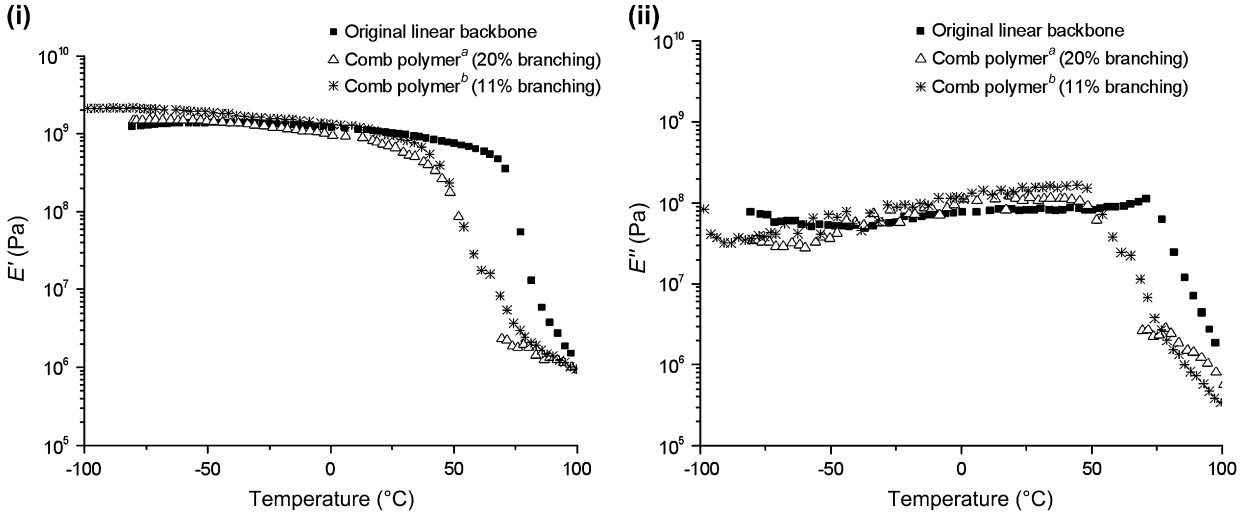

Fig. 12. Temperature dependence of (i) storage (E') and (ii) loss (E'') moduli of comb polymers with different amounts of branching. Original linear backbone poly(BMA-*co*-NAS) with $\overline{M}_n = 9.5 \times 10^4$, (a) poly(BMA-*co*-NAS-*graft*-BMA) containing 20% branching with branch $\overline{M}_n = 2.5 \times 10^4$ and (b) poly(BMA-*co*-NAS-*graft*-BMA) containing 11% branching with branch $\overline{M}_n \sim 2.5 \times 10^4$.

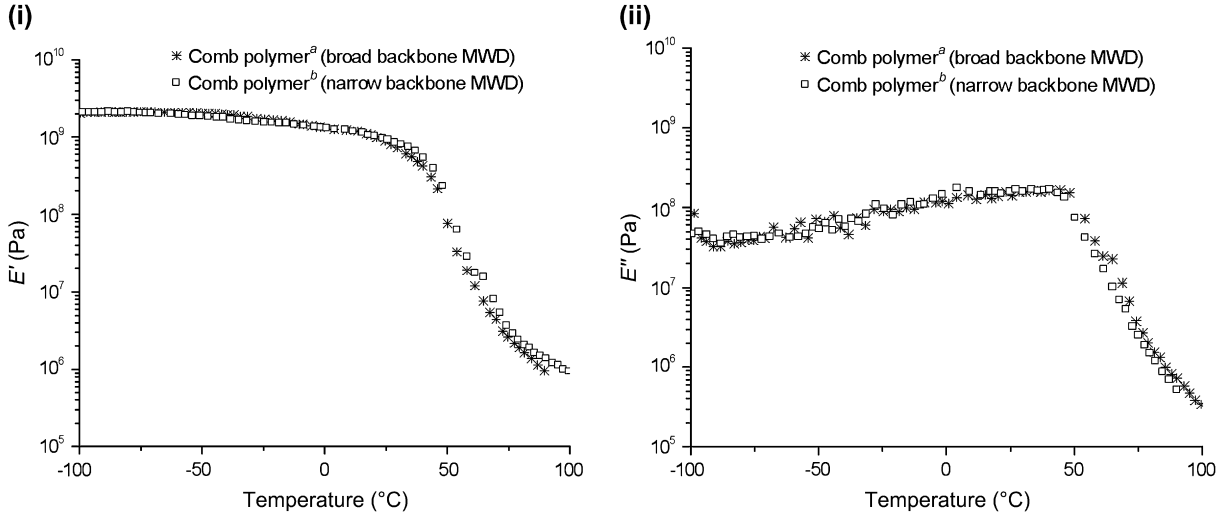

Fig. 13. Temperature dependence of (i) storage (E') and (ii) loss (E'') moduli of comb polymers differing with respect to molecular weight distribution of the backbone. (a) Backbone $\overline{M}_n = 9.5 \times 10^4$, PDI = 1.32, branch $\overline{M}_n = 9.9 \times 10^3$ and (b) backbone $\overline{M}_n = 57\,200$, PDI = 1.71, branch $\overline{M}_n \sim 9000$.

because of the applied strain. The storage and loss moduli of the comb polymers were consistently higher than those of the linear polymers, up to the point where the comb polymers started softening. The values of the storage and loss moduli for the different comb polymer series were very similar at the frequency (1 Hz) at which the temperature sweeps were conducted.

Frequency sweeps over a wide frequency range, constructed by time–temperature superpositioning, enabled a useful comparison of the mechanical properties of the different comb polymers. Master curves for the storage moduli of the different comb polymers are shown in Figs. 14–16. The storage moduli of the linear and comb polymers showed excellent superpositioning in all cases. This was not always the case for the loss moduli, because of the lower (~2 orders of magnitude) absolute values and subsequent larger contribution of noise.

Fig. 14 shows the effect of branch length on the storage moduli of the comb polymers. One sees a steady decrease in E' for the original linear polymer chains with decreasing frequency. The comb polymers exhibited a steady decrease in E' initially, followed by a rapid drop at lower frequencies. The steady decrease in E' for the linear polymers (and initially for the combs) can be ascribed to the local Rouse-like relaxations, i.e. very small localized motions for entities such as chain ends and small segments, or even parts of segments. The ensuing rapid decrease in E' of the combs can be ascribed to branch retraction out of the polymer matrix towards the comb backbone. This rapid decrease in E' was expected to occur earlier for the combs that contained shorter branches,

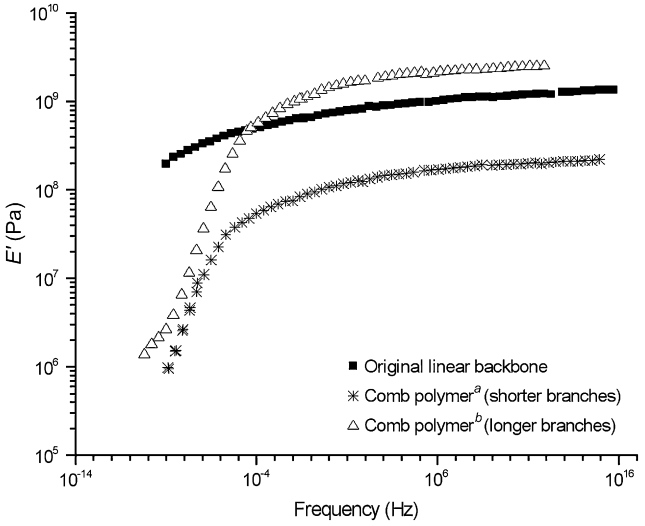

Fig. 14. Master curves showing storage modulus (E') for a comb polymer series differing only with respect to branch length. Original linear backbone poly(BMA-*co*-NAS) with $\overline{M}_n = 9.5 \times 10^4$, (a) poly(BMA-*co*-NAS-*graft*-BMA) with branch $\overline{M}_n = 9.9 \times 10^3$ and (b) poly(BMA-*co*-NAS-*graft*-BMA) with branch $\overline{M}_n = 2.5 \times 10^4$.

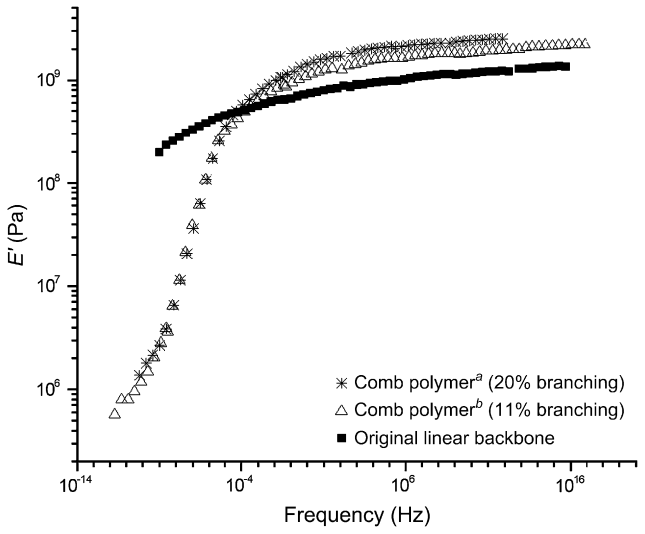

Fig. 15. Master curves showing storage modulus (E') for a comb polymer series differing only with respect to amount of branching. Original linear backbone poly(BMA-*co*-NAS) with $\overline{M}_n = 9.5 \times 10^4$, (a) poly(BMA-*co*-NAS-*graft*-BMA) containing 20% branching with branch $\overline{M}_n = 2.5 \times 10^4$ and (b) poly(BMA-*co*-NAS-*graft*-BMA) containing 11% branching with branch $\overline{M}_n \sim 2.5 \times 10^4$.

because of the smaller range of relaxation times associated with shorter branches compared to longer branches. The shorter branches therefore relax faster than the longer branches, leading to the rapid decrease in E' occurring at higher frequencies. The expected earlier onset, however, was not detected. At lower frequencies, when all the branches have relaxed, the comb backbone behaves as if effectively "dissolved" in the relaxed branches [10,11]. The comb backbone is now surrounded by a very large number of highly mobile chain ends, which in turn causes a significant dilation

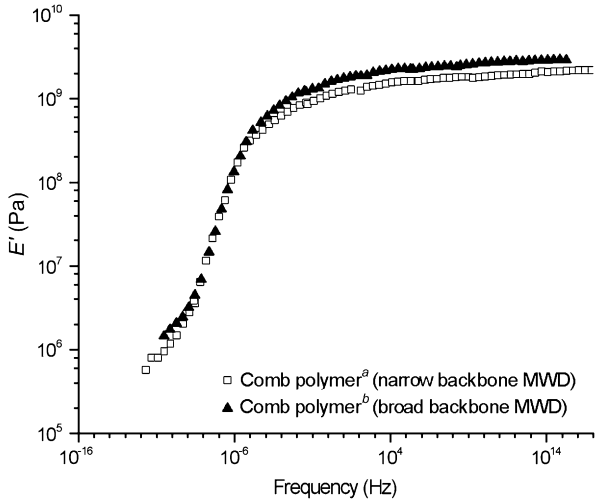

Fig. 16. Master curves showing the effect of molecular weight distribution of the comb backbone on E'. (a) Backbone $\overline{M}_n = 9.5 \times 10^4$, PDI = 1.32, branch $\overline{M}_n \sim 2.5 \times 10^4$ and (b) backbone $\overline{M}_n = 57\,200$, PDI = 1.71, branch $\overline{M}_n \sim 2.5 \times 10^4$.

of the effective tube [42] in which the linear backbone reptates.

The major difference between the E' of the combs and linear polymers at lower frequencies can thus be understood in terms of the abundance of relaxed chains and mobile chain ends as follows. The original linear polymers have two chain ends per molecule. At lower frequencies, the mobility of these chain ends steadily increases and E' therefore steadily decreases. In contrast to this, a poly(BMA-*co*-NAS-*graft*-BMA) comb polymer consisting of a backbone of $\overline{M}_n = 9.5 \times 10^4$ that contains 20% branching (i.e. a statistical average of one branch per five repeat units in the backbone), will contain approximately 136 chain ends. The slightly higher values for E' at very high frequencies for the combs with the longer branches are probably due to the higher degree of matrix entanglement and subsequently imposed constraints that those combs experience when compared to the combs with shorter branches.

Fig. 15 shows the effect of amount of branching on the storage moduli of the comb polymers. The same trends for E' are observed here as was the case in Fig. 14. The rapid decrease in E' occurs at roughly the same point for the two different combs, since the branch lengths were similar. At higher frequencies, the combs with fewer branches exhibited a slightly lower E'. The magnitude of the differences in moduli at high frequencies is probably well within the possible error associated with the measurements, but can still be explained in terms of the constraints imposed by branch points. At high frequencies, branch points are fixed in a molecule, thereby constraining Rouse-like motions of the branch segments close to the backbone. An increase in the number of branch points will therefore lead to an increase in segments subjected to these constraints, which in turn leads to an increase in E'.

Fig. 16 shows the effect of the molecular weight distribution of the comb backbone on E'. These data are consistent

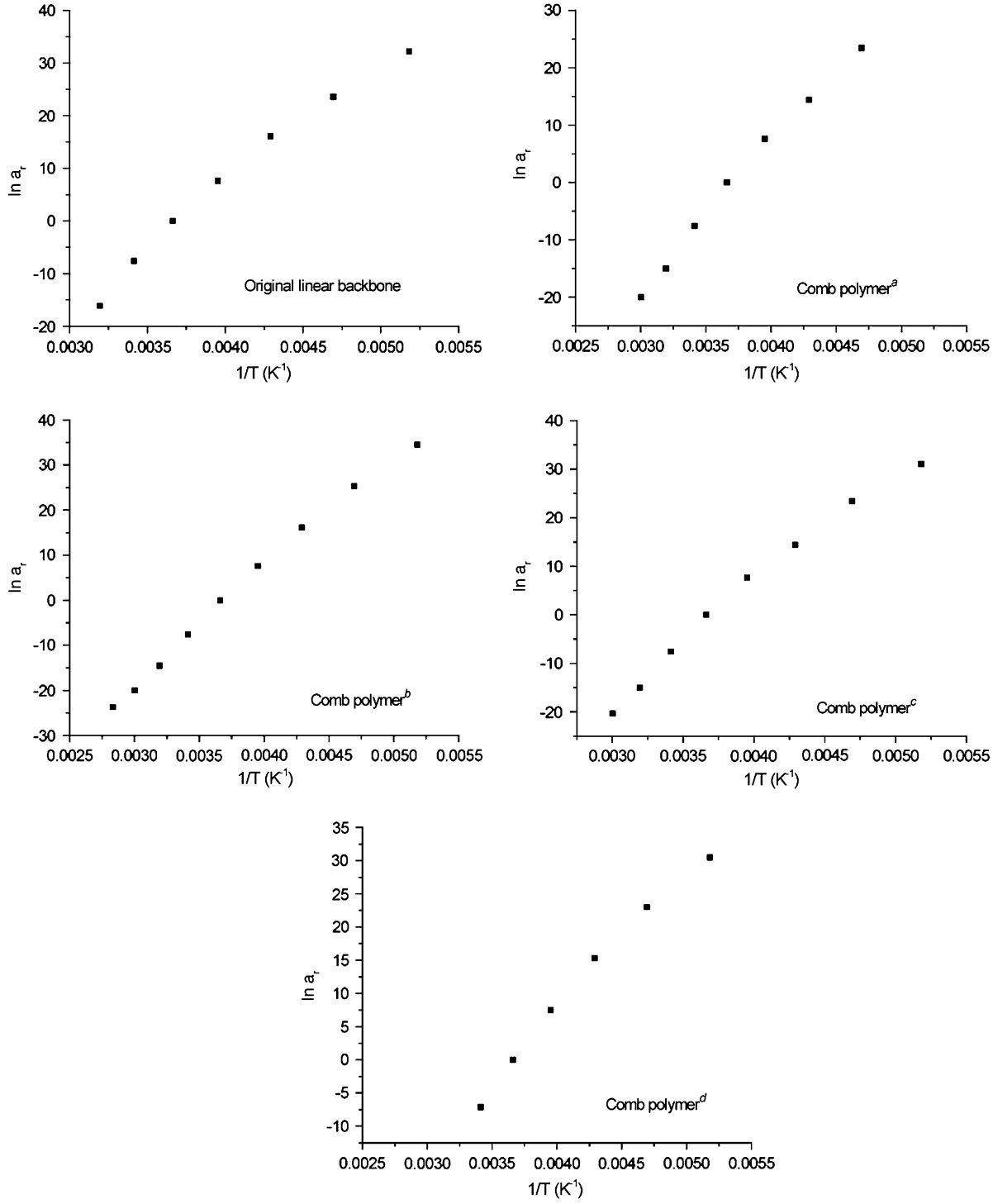

Fig. 17. Horizontal shift factors used for the different comb polymers. (a) Poly(BMA-*co*-NAS-*graft*-BMA) containing 20% branching with backbone $\overline{M}_n = 9.5 \times 10^4$, PDI = 1.32 and branch $\overline{M}_n = 2.5 \times 10^4$, (b) poly(BMA-*co*-NAS-*graft*-BMA) containing 11% branching with backbone $\overline{M}_n = 9.5 \times 10^4$, PDI = 1.32 and branch $\overline{M}_n \sim 2.5 \times 10^4$, (c) poly(BMA-*co*-NAS-*graft*-BMA) containing 7% branching with backbone $\overline{M}_n = 57\,200$, PDI = 1.71 and branch $\overline{M}_n \sim 2.5 \times 10^4$ and (d) poly(BMA-*co*-NAS-*graft*-BMA) containing 20% branching with backbone $\overline{M}_n = 9.5 \times 10^4$, PDI = 1.32 and branch $\overline{M}_n = 9.9 \times 10^3$.

with the DSC results shown earlier which showed that a backbone polydispersity index of 1.71 is not broad enough to make an impact on the mechanical properties of the polymers.

It is important to realize that in comb systems like these (with a high branching frequency, up to 20%), the branch motions completely dominate the material properties. Viscoelastic studies on combs reported in literature have been mostly conducted on combs that contained a very low number of branches per backbone (6–8 [43], 5–31 [44], 5–23 [11] and 30 branches [9]) whereas the combs considered here contained 46–136 branches per backbone chain. For example, in a polyBMA comb consisting of a backbone with

$\overline{M}_n = 9.5 \times 10^4$ and containing 20% branching with branch $\overline{M}_n = 2.5 \times 10^4$, the backbone only constitutes 2.8% of the molecular weight. This explains why subtle changes in modulus due to backbone reptation were not observed. These changes in moduli will be completely masked by the broad changes in moduli due to branch retractions.

Finally, since the arbitrary reference temperature (0 °C) used for TTS was below the glass transition temperature of the polymers, it was expected that the shift factors (a_T) should exhibit an Arrhenius-like dependence on temperature. It must be noted that the different temperature dependencies (Arrhenius and WLF) of the shift factors are completely based on empirical experimental observations. Fig. 17 shows the temperature dependence of the shift factors used to perform the time–temperature superposition of E' for the different comb polymers and original linear polymers. Fig. 17 also shows an approximately linear relationship between $\ln a_T$ and $1/T$ for all of the comb polymers under investigation as well as the original linear backbone polymers. The curvature at the low temperature region of the plots can arise from the subjective nature of the shifting procedure, or simply because there is no single activation barrier to the dynamical process. Indeed, this somewhat non-Arrhenius behavior for relatively monodisperse samples is not unusual. The Arrhenius behavior which is frequently seen in the literature arises because the samples are of much higher polydispersity than the subject of the present work.

At low temperatures, virtually complete horizontal overlapping of adjacent E' data sets is observed. This results in greater freedom when choosing the values of the shift factors, when compared to choosing shift factors for the data sets obtained at higher temperatures.

4. Conclusions

Different series of comb-like poly(BMA-*co*-NAS-*graft*-BMA) enabled a systematic investigation of the effect of various structural parameters on the thermal and viscoelastic properties of these polymers. DSC measurements showed clear differences between the glass transition temperatures of the comb polymers and the original linear backbones. Within the different series of combs, a change in branch frequency was the only variable that made an impact on the glass transition temperature of the comb polymers. Comb polymers differing only with respect to branch lengths did not have significantly different glass transition temperatures with respect to each other, neither did comb polymers differing only with respect to the molecular weight distributions of the backbones. The small differences in glass transition temperatures between the different comb polymers were rationalized in terms of changes in free volume, steric hindrance of the system and finally that the comb polymers showed the same thermal properties as long chain poly(*n*-butyl methacrylate), effects arising from the crowded nature of the combs synthesized here.

The viscoelastic properties were investigated using DMA. The storage modulus of all the different combs showed excellent time–temperature superpositioning, which was used to construct master curves over wide frequency ranges. Major differences in the viscoelastic responses of the original linear backbones and the comb polymers were observed. These differences were explained in terms of arm retraction/relaxation leading to effective tube dilation. All comb polymers showed viscoelastic responses that are characteristic of combs, but differences in responses due to changes in branch length and number were difficult to detect. This was mainly due to the relatively high number of branches, whose retractions occurred over a broad frequency range, and thus dominated the observed changes in moduli, thereby possibly masking subtle differences in responses.

No attempt is made in the present paper to quantitatively model the data. Our data are for polymers which are relatively monodisperse in terms of both the backbone and branched chains, and both of these parameters have been systematically varied; thus these data should prove useful for quantitative tests of the various sophisticated models now appearing in the literature [45,46].

Acknowledgements

The support of an Australian Research Council Discovery and ARC LIEF grant are gratefully acknowledged. Stuart Thickett and Hollie Zondanos are also gratefully acknowledged for SEC analyses, and excellent discussions with Dr. Angus Gray-Weale on hydrodynamic volume are greatly appreciated. The Key Centre for Polymer Colloids was established and supported under the Australian Research Council's Research Centres Program.

References

[1] Moad G, Solomon DH. The chemistry of free radical polymerization. 2nd ed. Amsterdam: Elsevier; 2006.
[2] Rizzardo E, Chiefari J, Chong YK, Ercole F, Krstina J, Jeffery J, et al. Macromol Symp 1999;143:291.
[3] Matyjaszewski K, Davis TP, editors. Handbook of radical polymerization. Hoboken: Wiley-Interscience; 2002.
[4] Podzimek S, Vlcek T. J Appl Polym Sci 2001;82:454.
[5] Podzimek S, Vlcek T, Johann C. J Appl Polym Sci 2001;81:1588.
[6] Pasch H. Macromol Symp 2002;178:25.
[7] Williams ML, Landel RF, Ferry JD. J Am Chem Soc 1955;77:3701.
[8] Yurasova TA, McLeish TCB, Semenov AN. Macromolecules 1994;27:7205.
[9] Roovers J, Graessley WW. Macromolecules 1981;14:766.
[10] Daniels DR, McLeish TCB, Crosby BJ, Young RN, Fernyhough CM. Macromolecules 2001;34:7025.
[11] Lohse DJ, Milner ST, Fetters LJ, Xenidou M, Hadjichristidis N, Mendelson RA, et al. Macromolecules 2002;35:3066.
[12] Dekmezian AH, Weng WQ, Garcia-Franco CA, Markel EJ. Polymer 2004;45:5635.
[13] Hritcu D, Muller W, Brooks DE. Macromolecules 1999;32:565.
[14] Lamb D, Anstey JF, Fellows CM, Monteiro JM, Gilbert RG. Biomacromolecules 2001;2:518.
[15] Guerrini MM, Charleux B, Vairon JP. Macromol Rapid Commun 2000;21:669.
[16] Kawaguchi H, Isono Y, Tsuji S. Macromol Symp 2002;179:75.
[17] D'Agosto F, Charreyre M-T, Pichot C, Gilbert RG. J Polym Sci Part A Polym Chem 2003;41:1188.

[18] Chiefari J, Chong YK, Ercole F, Krstina J, Le TPT, Mayadunne RTA, et al. Macromolecules 1998;31:5559.
[19] Vosloo JJ, Tonge MP, Fellows CM, D'Agosto F, Sanderson RD, Gilbert RG. Macromolecules 2004;37:2371.
[20] Börner HG, Matyjaszewski K. Macromol Symp 2002;177:1.
[21] Jenkins AD, Tsartolia E, Walton DRM, Horskajenkins J, Kratochvil P, Stejskal J. Makromol Chem Macromol Chem Phys 1990;191:2511.
[22] Hua FJ, Liu B, Hu CP, Yang YL. J Polym Sci Part A Polym Chem 2002; 40:1876.
[23] Blomberg S, Ostberg S, Harth E, Bosman AW, Horn BV, Hawker CJ. J Polym Sci Part A Polym Chem 2002;40:1309.
[24] Niimi L, Serita K, Hiraoka S, Yokozawa T. J Polym Sci Part A Polym Chem 2002;40:1236.
[25] Li Z, Du QG, Yang YL, Lin MD. Macromol Chem Phys 2001;202:2314.
[26] Guo XP, Li ZA, Du QG, Yang YL, Lin MD. J Appl Polym Sci 2002;84: 2318.
[27] Quinn JF, Chaplin RP, Davis TP. J Polym Sci Part A Polym Chem 2002; 40:2956.
[28] Stenzel MH, Davis TP, Fane AG. J Mater Chem 2003;13:2090.
[29] Tsujii Y, Ejaz M, Sato K, Goto A, Fukuda T. Macromolecules 2001;34: 8872.
[30] Börner HG, Beers KL, Matyjaszewski K, Sheiko SS, Möller M. Macromolecules 2001;34:4375.
[31] Gaborieau M, Gilbert RG, Gray-Weale A, Hernandez JM, Castignolles P. Macromol Theory Simul, in press.
[32] Ward RM, Gao Q, de Bruyn H, Lamb DJ, Gilbert RG, Fitzgerald MA. Biomacromolecules 2006;7:866.
[33] Andreozzi L, Castelvetro V, Faetti M, Giordano M, Zulli F. Macromolecules 2006;39:1880.
[34] Frater DJ, Mays JW, Jackson C. J Polym Sci Part B Polym Phys 1997;35: 141.
[35] Gerle M, Fischer K, Roos SG, Müller AHE, Schmidt M, Sheiko SS, et al. Macromolecules 1999;32:2629.
[36] Percec V, Ahn C-H, Cho W-D, Jamieson AM, Kim J, Leman T, et al. J Am Chem Soc 1998;120:8619.
[37] Radke W, Mueller AHE. Macromolecules 2005;38:3949.
[38] Kostanski LK, Keller DM, Hamielec AE. J Biochem Biophys Methods 2004;58:159.
[39] Sun H. J Phys Chem B 1998;102:7338.
[40] Brandrup J, Immergut EH, Grulke EA, editors. Polymer handbook. New York: John Wiley & Sons; 1999.
[41] Lu X, Jiang B. Polymer 1991;32:471.
[42] de Gennes PG. J Chem Phys 1971;55:572.
[43] Islam MT, Juliani, Archer LA, Varshney SK. Macromolecules 2001;34: 6438.
[44] Daniels DR, McLeish TCB, Kant R, Crosby BJ, Young RN, Pryke A, et al. Rheol Acta 2001;40:403.
[45] Kapnistos M, Vlassopoulos D, Roovers J, Leal LG. Macromolecules 2005;38:7852.
[46] Jabbarzadeh A, Atkinson JD, Tanner RI. Macromolecules 2003;36:5020.